DOI: 10.1002/ejic.200900144

Syntheses, Crystal Structures and Adsorption Properties of Ultramicroporous Coordination Polymers Constructed from Hexafluorosilicate Ions and Pyrazine

Kazuhiro Uemura,*[a] Akihisa Maeda,[a] Tapas Kumar Maji,[b] Prakash Kanoo,[b] and Hidetoshi Kita[a]

Keywords: Microporous materials / Metal–organic frameworks / Adsorption / Copper / Zinc

Three novel coordination polymers based on M^{2+} (M = Cu, Zn), pyrazine (pyz) and the SiF_6^{2-} ion, $[Cu(SiF_6)(pyz)(H_2O)_2]_n$ (**1a**), $\{[Cu(SiF_6)(pyz)_3]\cdot 2H_2O\}_n$ (**1b** ⊃ $2H_2O$) and $\{[Zn(SiF_6)(pyz)_2]\cdot 2MeOH\}_n$ (**2** ⊃ 2MeOH), have been synthesized and characterized by single-crystal X-ray diffraction analyses. Compound **1a** forms straight one-dimensional chains of $–Cu(OH_2)_2–pyz–$, which are bridged by SiF_6^{2-} ions to produce two-dimensional sheets. Compound **1b** ⊃ $2H_2O$ forms straight two-dimensional sheets of $–Cu(pyz)_2–pyz–$ chains bridged by SiF_6^{2-} ions, where perpendicularly protruding pyz planes are stacked to produce a three-dimensional framework with 2.5×2.2 Å^2 pores. In compound **2** ⊃ 2MeOH, grids of $[Zn(pyz)_2]_n$ are bridged by SiF_6^{2-} ions axially coordinating to Zn^{2+} ions to produce an open three-dimensional framework. The 4.5×4.5 Å^2 pores in **2** ⊃ 2MeOH are surrounded by pyz panels, and they remain intact after removal of solvents to give $[Zn(SiF_6)(pyz)_2]_n$ (**2**). The permanent porosity of **2** was characterized by adsorption studies with solvent vapours such as MeOH (kinetic diameter 3.8 Å), EtOH (4.3 Å), *i*PrOH (4.7 Å) and Me_2CO (4.7 Å), showing a size-exclusive effect at around 4.7 Å. Furthermore, the H_2 adsorption/desorption isotherm of **2** at 77 K shows a sharp uptake with a slight hysteresis loop, which is attributed to both the small size of the pore and the interaction between H_2 molecules and fluorine (SiF_6^{2-}) atoms that are exposed on the pore surfaces.

Introduction

The synthetic investigation of porous coordination polymers has been accelerated by the suggestion of reticular synthesis based on secondary building units (SBUs),[1] and numerous porous coordination polymers have been reported.[1–6] Because of their regulated porosities, researchers have identified several uses for this promising material, especially for gas separation and H_2 adsorption, in the last few years.[7–11] Focusing on gas separation, size-exclusive effects within porous materials have played an important role in their separation functions, whereby smaller molecules can go through the microporous channels whereas larger substrates are blocked. For example, $[Zn_2(BDC)_2(4,4'\text{-bpy})]_n$ (BDC = 1,4-benzenedicarboxylate, 4,4′-bpy = 4,4′-bipyridine) with 4.0×4.0 Å^2 cross-sectional channels shows highly selective gas-chromatographic separation of alkanes,[12] and $[VO(BDC)]_n$ (MIL-47),[13] having 10.5×11.5 Å^2 channels, also shows separation of C_8 alkyl aromatic compounds.[14] In addition, $[Zn(cbIM)_2]_n$ (ZIF-95, cbIM = 5-chlorobenzimidazole) with a 3.65 Å pore aperture is a good carbon dioxide reservoir, showing by a breakthrough curve that only CO_2 (kinetic diameter: 3.30 Å) is retained in the pores while N_2 (3.64 Å) passes through without hindrance.[15] As observed in the above examples, to achieve size-exclusive effects with porous coordination polymers, the window aperture size of the channels should be close to the size of the substrates that are expected to be separated.

H_2 storage is also one of the key technologies expected to result from research on porous coordination polymers, and much effort has focused on investigating this area in the past few years.[7–11] Although investigation of the extra large surface area, which is difficult to obtain by carbon or zeolite-type materials, has produced higher H_2 uptake,[16] there still remains room for strengthening physisorption by van der Waals interaction of H_2 molecules on porous materials. To strengthen adsorbate/framework interactions, two major approaches have been considered. One is pore surface engineering[17] by introduction of unsaturated metal centres into the pore surface[11] or increasing the polarizability of the organic struts.[18] The other is pore-shape and -size design, where small pores show a relatively high affinity for H_2.[19]

On the basis of this background, we reasoned that frameworks with ultramicropores (with pore sizes smaller than 7 Å) might well contribute to gas separation and yield novel

[a] Environmental Science and Engineering, Graduate School of Science and Engineering, Yamaguchi University,
Tokiwadai 2-16-1, Ube-shi, Yamaguchi 755-8611, Japan
Fax: +81-836-85-9601
E-mail: kazu-u@yamaguchi-u.ac.jp
[b] Chemistry and Physics of Materials Unit, Jawaharlal Nehru Centre for Advanced Scientific Research,
Jakkur, Bangalore 560064, India

Supporting information for this article is available on the WWW under http://www.eurjic.org or from the author.

results on H_2 adsorption. Although several interpenetrated (interwoven) frameworks[12,20–29] produce uniquely shaped pores in this size range, rational syntheses with reticular regulation have some difficulties because of the influence of ligand lengths. As shown in Scheme 1, typical bridging ligands, BDC and 4,4′-bpy, produce open octahedral coordination polymers, $[Zn_2(BDC)_2(dabco)]_n$ (dabco = 1,4-diazabicyclo[2.2.2]octane)[30] and $[Cu(SiF_6)(4,4'\text{-bpy})_2]_n$[31] with micropores of 7.5×7.5 Å^2 and 8.0×8.0 Å^2, respectively. For separation and purification of smaller gas molecules, such micropores need to be further narrowed to become ultramicropores, as in Prussian blue ($M(CN)_2$) analogues.[32,33] When we focus on SiF_6^{2-}-containing coordination compounds, $[M(SiF_6)(4,4'\text{-bpy})_2]_n$ (M = Zn^{2+}, Cu^{2+}),[31,34–36] which are compounds that can be regarded as having been generated from square-grid coordination polymers that are cross-linked by μ-SiF_6 anions, replacing 4,4′-bpy by pyrazine (pyz) would produce the required ultramicropores. Herein, we show the synthesis and characterization of ultramicroporous coordination polymers with formulae $[M(SiF_6)(pyz)_2]_n$ employed for gas and vapour adsorption studies and especially H_2 storage properties.

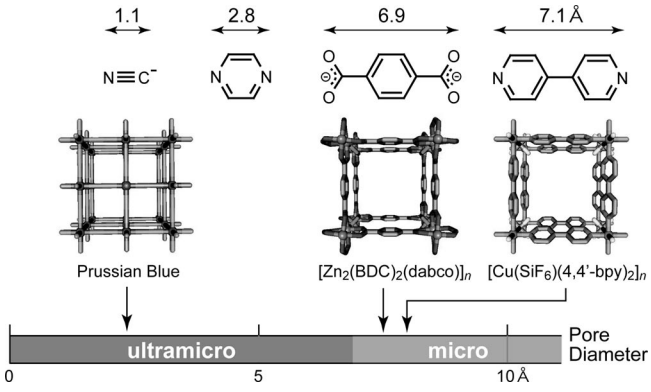

Scheme 1. Relationship between bridging ligand lengths and pore diameters found in porous coordination polymers.

Results and Discussion

Synthesis and Crystal Structures of $[Cu(SiF_6)(pyz)(H_2O)_2]_n$ (1a), $\{[Cu(SiF_6)(pyz)_3]\cdot 2H_2O\}_n$ (1b ⊃ $2H_2O$) and $\{[Cu_2(pyz)_3](SiF_6)\}_n$ (1c)

A compound with formula $[Cu(SiF_6)(pyz)(H_2O)_2]_n$ (**1a**) was obtained by following the synthetic procedure for $\{[Cu(SiF_6)(4,4'\text{-bpy})_2]\cdot 8H_2O\}_n$[31] by mixing the starting materials, $Cu(BF_4)_2\cdot xH_2O$, pyz and $(NH_4)_2SiF_6$, in water in the ratio 1:2:1 at room temperature, which immediately produced a blue precipitate. As time passed, the colour of the precipitate changed from blue to violet.[37] This colour change indicates that the blue compound is kinetically stable, whereas the violet compound is thermodynamically stable in this system.[38] As mentioned in the Experimental Section, we succeeded in obtaining single crystals of both the blue and the violet compounds, $[Cu(SiF_6)(pyz)(H_2O)_2]_n$ (**1a**) and $\{[Cu(SiF_6)(pyz)_3]\cdot 2H_2O\}_n$ (**1b** ⊃ $2H_2O$).

Figure 1 shows the coordination environment of the copper ion in **1a**. The copper(II) centre is octahedrally coordinated to the two nitrogen atoms of the pyz ligands and two water molecules in a trans fashion with Cu(1)–N(1) distances of 2.031(2) Å and Cu(1)–O(1) distances of 1.952(2) Å. In addition, two fluorine atoms of SiF_6^{2-} are coordinated axially with a Cu(1)–F(1) bond length of 2.4121(16) Å. In **1a**, the copper(II) ions are linked by pyz ligands to form straight one-dimensional chains, which are bridged by SiF_6^{2-} ions to produce a two-dimensional sheet (Figure 1b). The closest Cu–Cu distance is about 6.8 Å in the chain and 7.8 Å between adjacent chains. Each sheet stacks along the (a + c) direction and is bound by hydrogen bonds between coordinated water molecules and SiF_6^{2-} anions; $d[O(H_2O)\text{–}F(SiF_6^{2-})]$ = 2.63 Å.

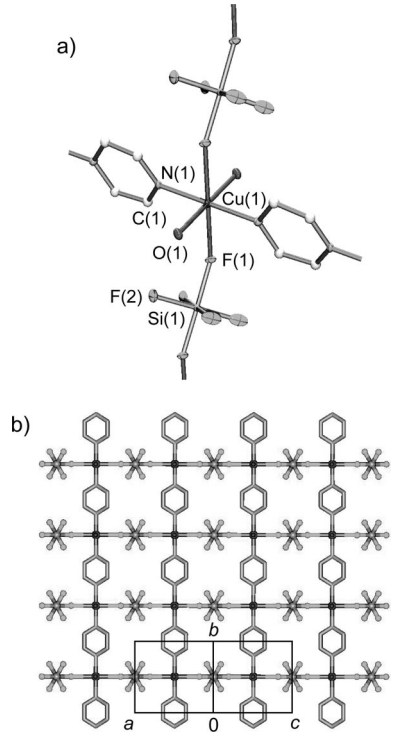

Figure 1. Crystal structure of $[Cu(SiF_6)(pyz)(H_2O)_2]_n$ (**1a**). (a) ORTEP drawing of **1a** at the 30% probability level. Hydrogen atoms are omitted for clarity. (b) Overall structure of **1a**. One-dimensional chains run in parallel to form a sheet, where SiF_6^{2-} anions bridge chains.

Figure 2 shows the coordination environment of the copper ion in $\{[Cu(SiF_6)(pyz)_3]\cdot 2H_2O\}_n$ (**1b** ⊃ $2H_2O$). The copper(II) centre is octahedrally coordinated to the four nitrogen atoms of the pyz ligands and the two SiF_6^{2-} groups. In the equatorial plane, all of the Cu–N bond lengths are similar to each other: Cu–N(1) 2.048(3) Å, Cu–N(2) 2.009(12) Å and Cu–N(4) 2.054(11) Å. One of the coordinated pyz ligands serves as a bridging ligand to produce a one-dimensional chain with a Cu–Cu distance of 6.9 Å, while the other forms side arms of one-dimensional chains acting as monodentate ligands. As shown in Figure 2b, the

one-dimensional arrays run in parallel along the *a* axis, where protruding pyz planes are stacked above each other with a 3.5 Å separation. In addition, the SiF_6^{2-} ions are coordinated axially [Cu–F(1) 2.402(3) Å], and the bridged copper ions have a Cu–Cu distance of 8.3 Å. As shown in Figure 2c, channels along the *a* axis with a cross-sectional area of 2.5 × 2.2 Å^2[39] are formed, which are occupied by water molecules. This structure is similar to the network motif of $\{[Cd(4,4'\text{-bpy})_3(H_2O)_2](NO_3)_2\cdot 2(4,4'\text{-bpy})\cdot 4.5H_2O\}_n$[40] and $\{[Cu(2\text{-py}SO_3)_2(4,4'\text{-bpy})]\cdot H_2O\}_n$ (2-pySO_3 = 2-pyridinesulfonate),[41] and the interdigitated fashion of $\{[Zn_2(ip)_2(4,4'\text{-bpy})_2]\cdot DMF\}_n$ (H_2ip = isophthalic acid).[42]

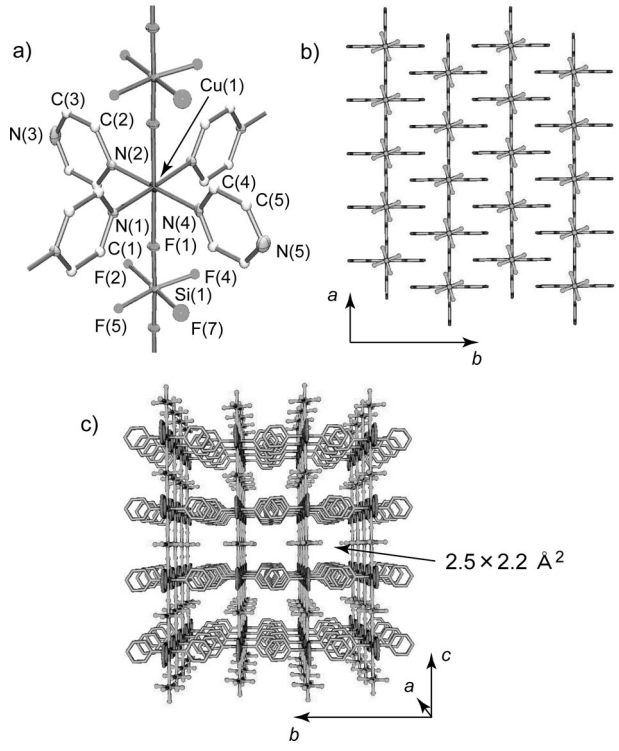

Figure 2. Crystal structure of $\{[Cu(SiF_6)(pyz)_3]\cdot 2H_2O\}_n$ (**1b** ⊃ $2H_2O$). (a) ORTEP drawing of **1b** ⊃ $2H_2O$ at the 30% probability level. F(3), F(6) and hydrogen atoms are omitted for clarity. (b) Overall structure of **1b** ⊃ $2H_2O$ along the *c* axis. Two-dimensional sheets run in parallel, where the pyridine planes are stacked to form the three-dimensional structure. (c) Cross sectional view along the *a* axis. The 2.5 × 2.2 Å pores are formed. Water molecules filling the pores are omitted for clarity.

Although the starting materials were mixed according to the synthetic procedure for $\{[Cu(SiF_6)(4,4'\text{-bpy})_2]\cdot 8H_2O\}_n$,[31,36] the expected structure, in which pyz ligands are incorporated in place of 4,4′-bpy ligands, was not obtained. This is because the pK_a value for pyz (0.65) is much smaller than that for 4,4′-bpy (4.44).[43] To promote the reaction, the mixed blue solution was heated to 120, 150 and 180 °C in a Teflon autoclave for 24 h. Although only light green solutions were obtained at 120 and 150 °C, orange crystals suitable for X-ray analysis were obtained at 180 °C. Single-crystal X-ray diffraction analysis showed that the orange crystal is $\{[Cu_2(pyz)_3](SiF_6)\}_n$ (**1c**), which has been previously reported.[44] In **1c**, the oxidation state of the copper ion is +1, indicating that the starting Cu^{II} ions are reduced to Cu^{I}. Such a reduction is probably induced by the Gillard mechanism,[45,46] where the attack by nucleophiles at the 2-position in complexed pyridine ligands (py) induces the reduction of the coordinated metal with release of H^+ and H_2O_2 species.[45] Actually, the pH of the supernatant solution of **1c** is 2.1, suggesting that high temperature promotes this pathway in our case. This mechanism also might be applicable for providing several Cu(I/II) mixed-valence compounds[46–51] and Cu^{I} coordination polymers;[52–57] high temperatures with py–X–py-type ligands probably assist in the reduction of Cu^{II} to Cu^{I}.

Crystal Structures of $\{[Zn(SiF_6)(pyz)_2]\cdot 2MeOH\}_n$ (**2** ⊃ 2MeOH)

Simple mixing of $ZnSiF_6\cdot xH_2O$ and pyz in MeOH solution produced colourless single crystals, which formed the expected crystal structure. Figure 3a shows the coordination environment of the zinc ion in $\{[Zn(SiF_6)(pyz)_2]\cdot 2MeOH\}_n$ (**2** ⊃ 2MeOH). The zinc(II) centre is octahedrally coordinated to the four nitrogen atoms of the pyz ligands and to the two SiF_6^{2-} ions. In the equatorial plane, the pyz ligands bridge the zinc ions [Zn–N(1) 2.172(5) Å] to produce grids with the closest Zn–Zn distance of 7.1 Å. In addition, the SiF_6^{2-} groups are coordinated axially [Zn–F(1) 2.057(5) Å] and bridge zinc ions with a Zn–Zn distance of 7.6 Å, producing an open three-dimensional framework (Figure 3b). As shown in Figure 3c, all pyz planes are paral-

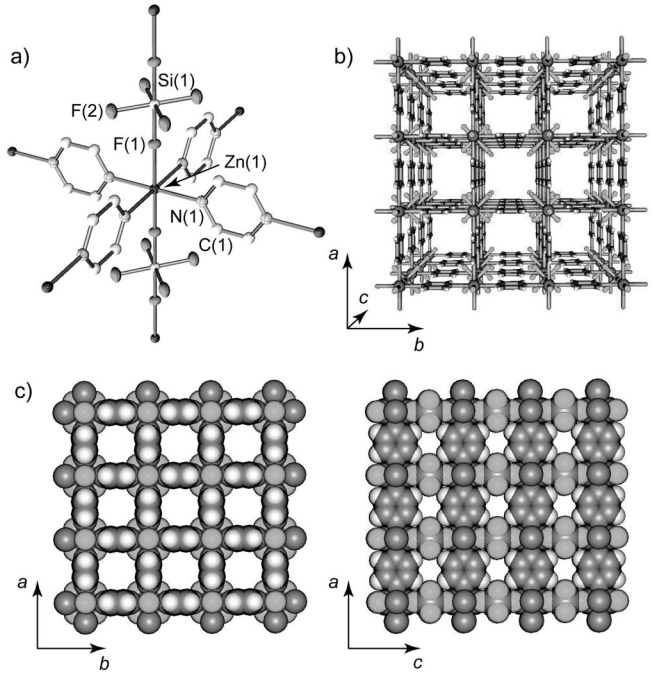

Figure 3. Crystal structure of $\{[Zn(SiF_6)(pyz)_2]\cdot 2MeOH\}_n$ (**2** ⊃ 2MeOH): (a) ORTEP drawing of **2** ⊃ 2MeOH at the 30% probability level. Hydrogen atoms are omitted for clarity. (b) Overall structure of **2** ⊃ 2MeOH along the *c* axis. (c) Space-filling view along the *c* axis (left) and the *b* axis (right). Pores of dimensions 4.5 × 4.5 Å^2 are formed.

Table 1. Comparison of distances and angles in selected coordination polymers containing bridging SiF_6^{2-} anions.

Compounds[a]	M	M–F(SiF_6^{2-}) distances/Å	M–N distances/Å	Canting angles/° [b]	Ref.
$[Co(SiF_6)(viz)_4]_n$	Co^{2+}	2.143(2)	2.097(2)	79.1	[66]
$[Cu(SiF_6)(4,4'\text{-bpy})_2]_n$	Cu^{2+}	2.355(5)	2.011(5)	63.9	[31]
$[Cu(SiF_6)(2,6\text{-}Me_2pyz)_4]_n$	Cu^{2+}	2.313(1), 2.83	2.023(1)	86.3	[67]
$\{[Cu(SiF_6)(pyz)_3]\cdot 2H_2O\}_n$ (**1b** ⊃ $2H_2O$)	Cu^{2+}	2.402(3)	2.009(12), 2.048(3), 2.054(11)	90.0	this work
$[Zn(SiF_6)(4,4'\text{-bpy})_2]_n$	Zn^{2+}	2.082(10)	2.157(8)	90.0	[34]
$\{[Zn(SiF_6)(bpp)_2]\cdot 4H_2O\cdot 2MeOH\}_n$	Zn^{2+}	2.135(1)	2.145(2), 2.170(2)	90.0	[68]
$\{[Zn(SiF_6)(4\text{-PDS})_2]\cdot 3MeOH\}_n$	Zn^{2+}	2.135(1)	2.007(4)–2.170(2)	73.4, 63.1	[69]
$\{[Zn(SiF_6)(pyz)_2]\cdot 2MeOH\}_n$ (**2** ⊃ 2MeOH)	Zn^{2+}	2.057(5)	2.172(5)	90.0	this work

[a] Abbreviations: viz. = *N*-vinylimidazole, 4,4′-bpy = 4,4′-bipyridine, 2,6-Me_2pyz = 2,6-dimethylpyrazine, pyz = pyrazine, bpp = 1,3-bis(4-pyridyl)propane, 4-PDS = 4,4′-dipyridyldisulfide. [b] Angles between *xy* coordination planes and coordinated pyridine planes.

lel to the *c* axis, to produce pores with a cross-sectional area of 4.5 × 4.5 Å^2 surrounded by pyz panels. In this structure, 30% of the total crystal volume is void space,[58] whereas $[Zn(SiF_6)(4,4'\text{-bpy})_2]_n$ contains 50% void space.[34]

In the case of several coordination polymers containing SiF_6^{2-} anions as guest molecules,[59–65] coordinated water or solvent molecules result in a network that is of low dimensionality and often forms no channels. On the other hand, using SiF_6^{2-} anions as bridging ligands raises the dimensionality; Table 1 summarizes MN_4F_2-type [coordination of four N donor atoms to M (metal)] coordination polymers containing bridging SiF_6^{2-} anions.[31,34,66–69] To the best of our knowledge, only three metals (Co^{2+}, Cu^{2+} and Zn^{2+}) have been used to construct these network motifs. Obviously, the distances between Cu^{2+} and F(SiF_6^{2-}) are longer than those found in Co^{2+} or Zn^{2+} compounds, and Jahn–Teller distorted $[CuN_4F_2]$ coordination octahedra are formed in the Cu^{2+} compounds. Although the distances between M^{2+} and F(SiF_6^{2-}) are shorter (< 2.14 Å) in Co^{2+} and Zn^{2+} compounds, the orientation of the N donor ligands with respect to the *xy* coordination plane is almost perpendicular in order to avoid steric interactions with the SiF_6^{2-}. Also, in **2** ⊃ 2MeOH, the canting angle of the pyz ring relative to the *xy* coordination plane is zero, which contributes to the formation of effective 4.5 × 4.5 Å^2 open apertures.

Framework Stability of $\{[Zn(SiF_6)(pyz)_2]\cdot 2MeOH\}_n$ (**2** ⊃ 2MeOH)

The stability of the porous networks was studied by X-ray powder diffraction (XRPD) measurements and thermal gravimetric (TG) analysis. Figure 4a shows the thermogram of **2** ⊃ 2MeOH in the temperature range 20–300 °C for a heating rate β = 20 °C min^{-1}. In the temperature range 50–140 °C, the thermogram of **2** ⊃ 2MeOH showed a mass loss (observed = 15.3%) corresponding to guest molecules and then a gradual decomposition with loss of the SiF_6^{2-} ions and pyz ligands. The guests are considered to be two methanol molecules (calculated 14.8%) of solvent, although it is impossible to find them in **2** ⊃ 2MeOH by single-crystal X-ray diffraction analysis. Therefore, the formula containing guest molecules of **2** ⊃ 2MeOH is $\{[Zn(SiF_6)(pyz)_2]\cdot 2MeOH\}_n$ (**2** ⊃ 2MeOH). The XRPD pattern of dried $[Zn(SiF_6)(pyz)_2]_n$ (**2**), which was obtained by drying as-prepared **2** ⊃ 2MeOH in vacuo at 100 °C for 1 h, shows sharp peaks at similar peak positions as **2** ⊃ 2MeOH, indicating that compound **2** maintains its framework after removal of the MeOH molecules.

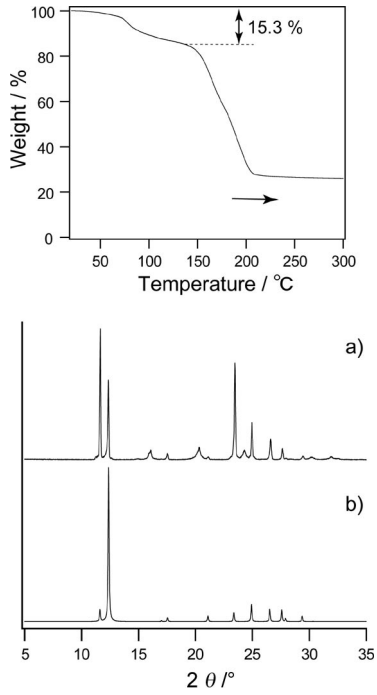

Figure 4. TG analysis of $\{[Zn(SiF_6)(pyz)_2]\cdot 2MeOH\}_n$ (**2** ⊃ 2MeOH) over the temperature range from 20 to 300 °C in a helium flow (100 mL min^{-1}). Heating rate: 20 °C min^{-1}. XRPD patterns of (a) drying **2** ⊃ 2MeOH in vacuo at 100 °C for 1 h (**2**) and (b) powder simulation of **2** ⊃ 2MeOH based on single-crystal X-ray diffraction analysis.

Adsorption Measurements of $[Zn(SiF_6)(pyz)_2]_n$ (**2**)

Three-dimensional porous coordination polymer **2** is useful for the adsorption of several gases. A N_2 (kinetic diameter: 3.64 Å) adsorption experiment was carried out over the pressure range from 0.035 to 0.993 atm at 77 K, as shown in Figure 5. The adsorption isotherm displays a rapid rise at low relative pressure followed by a monotonically increasing curve. Compound **2** adsorbs 146 cm^3 g^{-1} of N_2 at

77 K and 0.993 atm, corresponding to apparent Brunauer–Emmett–Teller (BET) and Langmuir surface areas of 133 and 217 $m^2 g^{-1}$, respectively. These surface areas are smaller than expected on the basis of the crystal structure, a fact that is attributed to the small amounts of adsorption at low relative pressure. Despite the stable framework and a larger pore diameter, effective N_2 diffusion into the micropores was not observed. The reason is the strong interaction of the N_2 molecules with the pore windows, which subsequently block other molecules from passing into the pore,[23] as is usually observed in other porous coordination polymers.[24,27,28,70–76]

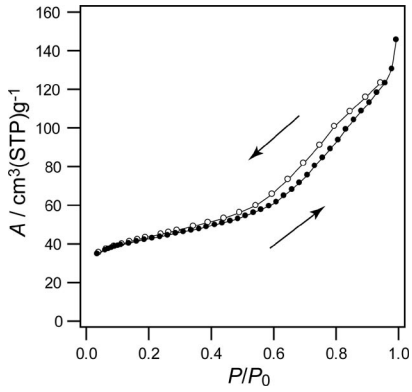

Figure 5. N_2 adsorption (filled circles) and desorption (open circles) isotherms at 77 K for $[Zn(SiF_6)(pyz)_2]_n$ (**2**) over the pressure range from 0.035 to 0.993 atm. P_0 is the saturation vapour pressure of N_2 at 77 K.

Figure 6 shows MeOH (kinetic diameter:[77] 3.8 Å), EtOH (4.3 Å), *i*PrOH (4.7 Å) and Me_2CO (4.7 Å) adsorption isotherms for **2** at 298 K. In spite of the difference in saturation amounts among the adsorbates, all isotherms show type-I curves, which are indicative of typical micropores. Because the adsorbate sizes are larger, the saturation amounts decrease. Table 2 summarizes the values of saturation amounts (W_0) and adsorption energy related to the adsorbate–adsorbent interaction (βE_0) based on the Dubinin–Radushkevich (DR) equation.[78,79] The noteworthy feature found in the isotherms is that **2** adsorbs Me_2CO rather than *i*PrOH. These results suggest that **2** may behave as a highly effective size-selective molecular sieve that can discriminate, for example, between *i*PrOH and Me_2CO or *i*PrOH and EtOH.

To further clarify the adsorption of gaseous solvent, we analyzed the adsorption phenomenon from a kinetic point of view. Figure 7 shows how adsorption reaches equilibrium from measurements on each solvent, calculated on the basis of pressure decays, where M_t and M_e are the mass uptake at time t and at equilibrium, respectively. In these volumetric measurements, the pressure change is proportional to the adsorption volume. Within these structures, there are barriers as a result of diffusion both through the windows and along the pore cavities. Although these can be described by a double-exponential (DE) equation,[80,81] the kinetic profiles for MeOH, EtOH, *i*PrOH and Me_2CO adsorption on **2** do not follow the DE model. However, the time t required

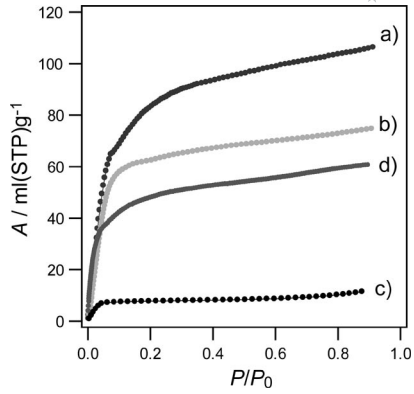

Figure 6. Adsorption isotherms for (a) MeOH, (b) EtOH, (c) *i*PrOH and (d) Me_2CO at 298 K for $[Zn(SiF_6)(pyz)_2]_n$ (**2**) over the relative pressure range from 0 to 0.9. P_0 is the saturation vapour pressure at 298 K: 16.913 (MeOH), 7.887 (EtOH), 5.930 (*i*PrOH) and 30.816 (Me_2CO) kPa.

Table 2. Calculated W_0 (mL(STP) g^{-1}) and βE_0 (kJ mol^{-1}) based on adsorption isotherms of **2**.

Adsorbate	W_0 /mL(STP) g^{-1}	βE_0 /kJ mol^{-1}
MeOH	100.6	9.3
EtOH	69.3	12.9
*i*PrOH	8.0	21.2
Me_2CO	54.6	11.4

for *i*PrOH to reach equilibrium is obviously longer than that for other solvents, indicating that *i*PrOH interacts very strongly with the pore windows, thereby blocking other molecules from passing into the pore, as the framework has no other additional open channel.

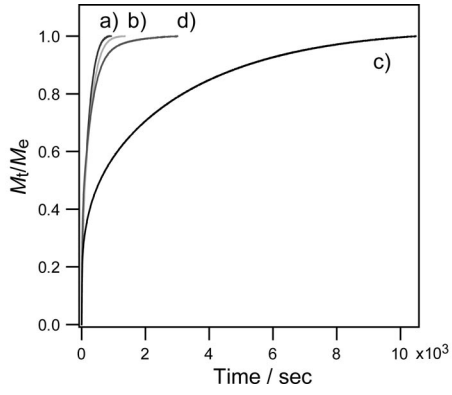

Figure 7. A comparison of adsorption kinetic profiles for M_t/M_e vs. time for the adsorption of MeOH, EtOH, *i*PrOH and Me_2CO on **2**: (a) MeOH (P = 0.0000–0.0388 kPa); (b) EtOH (P = 0.0000–0.0139 kPa); (c) *i*PrOH (P = 0.0000–0.0263 kPa); (d) Me_2CO (P = 0.0000–0.0124 kPa).

In addition, a measurement of H_2 (kinetic diameter: 2.89 Å) adsorption/desorption on **2** was carried out in the range 0–100 bar at 77 and 298 K (Figure 8). The adsorption isotherm at 77 K shows a sharp increase at low pressures and then slightly increases towards saturation, showing uptakes of 0.65 wt.-% [73.4 cm^3(STP) g^{-1}] and 1.09 wt.-% [123.4 cm^3(STP) g^{-1}] at 1.0 and 100 bar, respectively. Consequently, one pore, which is defined as the volume of a rect-

angle surrounded by eight Zn corners, could contain 2.0 H_2 molecules at 100 bar. The density of H_2 stored in the cavities of **2** is 0.018 molecules $Å^{-3}$, which is close to that of liquid H_2 (0.021 molecules $Å^{-3}$).[76] In contrast, the adsorption isotherm at 298 K shows a monotonic increase with an uptake of 0.14 wt.-% [16.1 $cm^3(STP)\,g^{-1}$] at 102 bar, where the adsorption data follow the Langmuir equation closely and predict a saturation of 0.40 wt.-% [44.8 $cm^3(STP)\,g^{-1}$],[82] indicating that additional H_2 molecules could be adsorbed at higher pressure. The isosteric heat of adsorption at zero coverage for **2** is 8.2 $kJ\,mol^{-1}$, calculated from the adsorption isotherms at 77 and 298 K. The significant feature is that the desorption isotherms do not retrace the adsorption isotherms, instead they show hysteresis.[83] There is the possibility that the slight hysteresis in H_2 adsorption/desorption on **2** is attributed to the relatively high isosteric heat of adsorption.

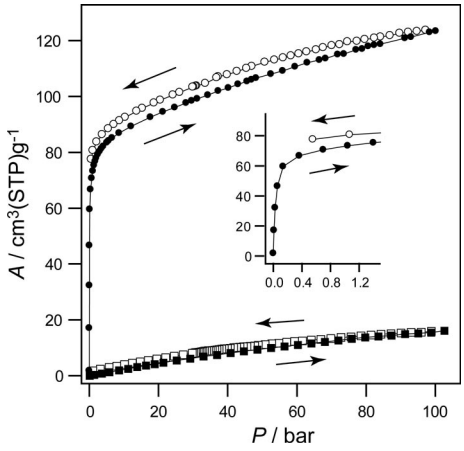

Figure 8. Isotherm for H_2 adsorption (filled) and desorption (open) on $[Zn(SiF_6)(pyz)_2]_n$ (**2**) at 77 (circles) and 298 (squares) K. The inset is a magnification of the 77 K isotherm.

The hysteresis in H_2 adsorption/desorption on porous coordination polymers[12,24–27,74,76,84–89] is classified into two types: small pores[74,76,87] and flexible pores.[12,24–27,84–86] In the former type, the small pores hinder diffusion of the H_2 molecules through ultramicropores of comparable size, because the interaction potential of the H_2 molecules is expected to be very strong due to the synergistic effect of the neighbouring pore walls.[19,76] Such a strong interaction leads to slow adsorption kinetics, resulting in adsorption/desorption hysteresis. On the other hand, in flexible pores, the hysteresis is attributed to additional steric hindrance caused by adjacent guests (kinetic trapping), where such slow desorption kinetics might be the result of the high H_2 loading of the porous framework at low pressures, which impedes the flexibility and window opening.[85] It is likely that the former small pore mechanism operates in the hysteresis described here, because **2** keeps its robust framework. In addition, taking into account the reports that $[Cu(hfipbb)(H_2hfipbb)_{0.5}]_n$ [H_2hfipbb = 4,4-(hexafluoroisopropylidene)bis(benzoic acid)] with 5.1×5.1 $Å^2$ ultramicrochannels[87] and $\{Ag_2[Ag_4Tz_6]\}_n$ [Tz = 3,5-bis(trifluoromethyl)1,2,4-triazolate] with 6.6×4.9 $Å^2$ ultramicrochannels show hysteresis, there is the possibility that interactions between H_2 molecules and fluorine atoms of SiF_6^{2-} are effective for trapping H_2 molecules in **2**. Although these results do not satisfy the standards set for practical applications, hysteretic adsorption could potentially lead to an effective means of H_2 storage.

Conclusions

This work was devoted to the syntheses of three coordination polymers prepared by using Cu^{2+} or Zn^{2+} (M = Cu, Zn), pyz and the SiF_6^{2-} ion to form ultramicroporous frameworks. Although the expected frameworks were not obtained by Cu^{2+} ions because of the low pK_a value of pyz and reduction of Cu^{2+} to Cu^+, we succeeded in obtaining porous coordination polymers by simply mixing $ZnSiF_6$ and pyz in MeOH. The ultramicropores (4.5×4.5 $Å^2$) of **2** show the size-exclusive effect and a sharp uptake in H_2 adsorption at 77 K, because the interaction potential is expected to be strong as a result of the synergistic effect of the neighbouring pore walls. We have, therefore, developed and contributed a series of SiF_6^{2-}-bridging porous coordination polymers with pyz that can be further narrowed down for ultramicropores.

Experimental Section

Materials: $Cu(BF_4)_2{\cdot}xH_2O$, $ZnSiF_6{\cdot}xH_2O$ and $(NH_4)_2SiF_6$ were obtained from Aldrich Chemical Co. Pyrazine was obtained from Tokyo Kasei Industrial Co.

$[Cu(SiF_6)(pyz)(H_2O)_2]_n$ (1a): To obtain the single crystals, an aqueous solution (2.0 mL) of pyz (0.36 g, 4.4 mmol) in a glass tube (5 mL, 10 mm i.d.) was carefully layered onto an aqueous solution (2.0 mL) of $Cu(BF_4)_2{\cdot}xH_2O$ (0.53 g, 2.2 mmol) and $(NH_4)_2SiF_6$ (0.40 g, 2.2 mmol). After two weeks, blue crystals of **1a** and violet crystals of **1b** $\supset 2H_2O$ were obtained at the bottom and the top of tube, respectively. By careful separation, blue crystals of **1a** suitable for X-ray diffraction were obtained (yield: 31%). $C_4H_8CuF_6N_2O_2Si$ (322): calcd. C 14.93, H 2.51, N 8.71; found C 14.09, H 2.17, N 8.75. The microcrystalline sample of **1a** was prepared in a dilute condition [pyz (0.36 g, 4.4 mmol), $Cu(BF_4)_2{\cdot}xH_2O$ (0.53 g, 2.2 mmol) and $(NH_4)_2SiF_6$ (0.40 g, 2.2 mmol) with H_2O (12 mL)]. After stirring for one day and placement for 12 h, a blue powder was obtained (yield: 5%). The crystallinity was checked by X-ray powder diffraction as shown in Figure S3 (Supporting Information).

$\{[Cu(SiF_6)(pyz)_3]{\cdot}2H_2O\}_n$ (1b $\supset$ 2H$_2$O): To obtain the single crystals, water (0.25 mL) in a glass tube (5 mL, 10 mm i.d.) was carefully layered onto an aqueous solution (1.25 mL) of $Cu(BF_4)_2{\cdot}xH_2O$ (0.48 g, 2.0 mmol) and $(NH_4)_2SiF_6$ (0.36 g, 2.0 mmol), and then an aqueous solution (1.25 mL) of pyz (0.32 g, 4.0 mmol) was carefully layered. After two weeks, violet crystals of **1b** $\supset 2H_2O$ suitable for X-ray diffraction were obtained (yield: 43%). $C_{12}H_{16}CuF_6N_6O_2Si$ (482): calcd. C 29.91, H 3.35, N 17.44; found C 30.04, H 2.76, N 17.84. The microcrystalline sample of **1b** $\supset$ $2H_2O$ was prepared with pyz (0.36 g, 4.4 mmol), $Cu(BF_4)_2{\cdot}xH_2O$ (0.53 g, 2.2 mmol) and $(NH_4)_2SiF_6$ (0.40 g, 2.2 mmol) with H_2O (10 mL). After stirring for one day, a violet powder was obtained

(yield: 22%). The crystallinity was checked by X-ray powder diffraction as shown in Figure S3 (Supporting Information).

{[Zn(SiF$_6$)(pyz)$_2$]·2MeOH}$_n$ (2 ⊃ 2MeOH): In order to obtain the single crystals, in a glass tube (5 mL, 10 mm i.d.) a methanol solution (2.0 mL) of pyz (0.10 g, 1.3 mmol) was carefully layered onto a methanol solution (2.0 mL) of $ZnSiF_6{\cdot}xH_2O$ (0.13 g, 0.6 mmol). Colourless crystals of **2** ⊃ 2MeOH suitable for X-ray diffraction were obtained (yield: 34%). $C_8H_{12}F_6N_4O_2SiZn$ (404): calcd. C 23.80, H 3.00, N 13.88; found C 23.29, H 2.09, N 13.87. Dried **2** is moisture sensitive, including H_2O in the pores.

X-ray Crystallographic Analysis: Single crystals of **1a**, **1b** ⊃ $2H_2O$ or **2** ⊃ 2MeOH were mounted on a glass fibre and coated with epoxy resin. X-ray data collection was carried out by using the imaging plate detector of a Rigaku RAXIS-RAPID diffractometer (**1a** and **1b** ⊃ $2H_2O$) or the CCD two-dimensional detector of a Rigaku Mercury diffractometer (**2** ⊃ 2MeOH) with graphite monochromated Mo-K_α radiation (λ = 0.7107 Å). For **1a** and **1b** ⊃ $2H_2O$, the sizes of the unit cells were determined from reflections collected on the setting angles of three frames by changing ω by 3.0° for each frame, and intensity data were collected with a ω scan width of 5.0°. For **2** ⊃ 2MeOH, the sizes of the unit cells were determined from reflections collected on the setting angles of six frames by changing ω by 0.5° for each frame, and intensity data were collected with a ω scan width of 0.5°. Two different χ settings were used. Empirical absorption correction[90] was performed for all data (Table 3). The structures were solved by the direct method with the subsequent difference Fourier syntheses and refinement with the SHELXTL (version 5.1) software package.[91] The non-hydrogen atoms were refined anisotropically, and all hydrogen atoms were placed in the ideal positions. In **1b** ⊃ $2H_2O$, the F2–7 atoms were isotropically refined with a disorder relationship, and water molecules (O1 and O2) were isotropically refined. CCDC-700685 (**1a**), -700686 (**1b** ⊃ $2H_2O$) and -700687 (**2** ⊃ 2MeOH) contain the supplementary crystallographic data for this paper. These data can be obtained free of charge from the Cambridge Crystallographic Data Centre via www.ccdc.cam.ac.uk/data_request/cif.

Physical Measurements: Thermal gravimetry (TG) was carried out with a Rigaku Instrument TG8120 in a helium flow (100 mL min^{-1}). IR spectra were recorded with a JASCO FTIR-610 spectrophotometer for which the samples were prepared with KBr. X-ray powder diffraction (XRPD) data were collected with a Rigaku RINT-2200YS diffractometer with Cu-K_α radiation. The N_2 (77 K) adsorption measurement was carried out in Quantachrome Autsorb-1. The adsorption isotherms of gaseous MeOH, EtOH, *i*PrOH and Me_2CO were measured by using BELSORP18-Plus volumetric adsorption equipment from BEL JAPAN. The adsorbent sample (≈ 100 mg), which had been prepared at 393 K and 10^{-1} Pa prior to measurement of the isotherms, was placed in the sample chamber (volume ≈ 19.5 mL) maintained at 298 ± 0.03 K. The larger gas chamber (176.51 mL) with a pressure gauge was kept at 318 ± 0.1 K. The saturation vapour pressures were calculated by using the following equation: $\log_{10}P = A - B/(T + C)$, where P is the saturation vapour pressure in Torr, T is the temperature in degrees Celsius, and A, B and C are constants defined by the adsorbate. MeOH: A = 8.07246, B = 1574.99, C = 238.86; EtOH: A = 8.21337, B = 1652.05, C = 231.48; *i*PrOH: A = 8.39424, B = 1730.00, C = 231.45; Me_2CO: A = 7.23967, B = 1279.87, C = 237.5.

Hydrogen Adsorption Measurements: High-pressure hydrogen sorption isotherm measurements at 77 and 298 K on **2** were carried out with a fully computer-controlled volumetric BELSORP-HP, BEL JAPAN high pressure instrument. The hydrogen used for the high pressure measurements is scientific/research grade with 99.999% purity. For the measurements, approximately 1.00 g sample was taken in a stainless steel sample holder and degassed at 120 °C for a period of 16 h under 0.1 Pa vacuum. The dead volume of the sample cell was measured with helium gas of 99.999% purity. Non-ideal correction for hydrogen gas was made by applying Virial coefficients at the respective measurement temperature.

Supporting Information (see footnote on the first page of this article): ORTEP drawing of **1b** ⊃ $2H_2O$ with disorder relationship (Figure S1); crystal structure of **1c** (Figure S2); XRPD patterns of prepared samples and simulation for **1a**, **1b** ⊃ $2H_2O$ and **1c** (Figure S3); IR spectra of **1a**, **1b** ⊃ $2H_2O$ and **1c** (Figure S4); BET and Langmuir plots based on N_2 adsorption at 77 K of **2** (Figure S5); adsorption/desorption isotherms and DR analyses on **2** for MeOH (Figure S6), EtOH (Figure S7), *i*PrOH (Figure S8) and Me_2CO (Figure S9); H_2 adsorption/desorption isotherms on **2** at 298 K

Table 3. Crystal data and structure refinement of $[Cu(SiF_6)(pyz)(H_2O)_2]_n$ (**1a**), $\{[Cu(SiF_6)(pyz)_3]{\cdot}2H_2O\}_n$ (**1b** ⊃ $2H_2O$) and $\{[Zn(SiF_6)(pyz)_2]{\cdot}2MeOH\}_n$ (**2** ⊃ 2MeOH).

Compound	**1a**	**1b** ⊃ $2H_2O$	**2** ⊃ 2MeOH
Chemical formula	$C_4H_8CuF_6N_2O_2Si$	$C_{12}H_{12}CuF_6N_6O_2Si$	$C_8H_8F_6N_4SiZn$
Formula weight	321.75	477.91	367.64
Crystal system	monoclinic	orthorhombic	tetragonal
Space group	*C*2/*m*	*Cm*2*m*	*P*4/*mmm*
Temperature/K	298	298	298
a/Å	10.737(2)	6.8879(14)	7.1409(10)
b/Å	6.8406(14)	16.140(3)	7.1409(10)
c/Å	7.7630(16)	8.2562(17)	7.6068(15)
α/°	90	90	90
β/°	128.12(3)	90	90
γ/°	90	90	90
V/Å^3	448.6(2)	917.8(3)	387.89(11)
Z	2	2	1
D_c/g cm^{-1}	2.382	1.729	1.574
μ(Mo-K_α)/mm^{-1}	2.655	1.335	1.716
2θ range/°	6.7–54.9	6.4–54.9	7.8–54.9
GOF on F^2	1.215	1.162	1.306
R_1[a] [$I > 2.0\sigma(I)$]	0.0239	0.0395	0.0498
wR_2[b] (all data)	0.0640	0.1242	0.1847

[a] $R_1 = \Sigma(|F_o| - |F_c|)/\Sigma(|F_o|)$. [b] $wR_2 = \{\Sigma[w(F_o^2 - F_c^2)^2]/\Sigma[w(F_o^2)^2]\}^{1/2}$.

(Figure S10); data for H_2 adsorption/desorption on **2** at 77 K (Table S1) and 298 K (Table S2).

Acknowledgments

This work was supported by the Grants-in-Aid for Scientific Research [Young Scientist (B) No. 17750058] and Mukai Science and Technology Foundation. T. K. Maji gratefully acknowledges the Department of Science and Technology, Govt. of India for the financial support (Fast track proposal).

[1] O. M. Yaghi, M. O'Keeffe, N. W. Ockwig, H. K. Chae, M. Eddaoudi, J. Kim, *Nature* **2003**, *423*, 705.
[2] S. L. James, *Chem. Soc. Rev.* **2003**, *32*, 276.
[3] C. Janiak, *Dalton Trans.* **2003**, 2781.
[4] S. Kitagawa, R. Kitaura, S.-i. Noro, *Angew. Chem. Int. Ed.* **2004**, *43*, 2334.
[5] G. Férey, C. Mellot-Dranznieks, C. Serre, F. Millange, *Acc. Chem. Res.* **2005**, *38*, 217.
[6] S. Kitagawa, K. Uemura, *Chem. Soc. Rev.* **2005**, *34*, 109.
[7] J. L. C. Rowsell, O. M. Yaghi, *Angew. Chem. Int. Ed.* **2005**, *44*, 4670.
[8] K. M. Thomas, *Catal. Today* **2007**, *120*, 389.
[9] G. Férey, *Chem. Soc. Rev.* **2008**, *37*, 191.
[10] R. E. Morris, P. S. Wheatley, *Angew. Chem. Int. Ed.* **2008**, *47*, 4966.
[11] M. Dincă, J. R. Long, *Angew. Chem. Int. Ed.* **2008**, *47*, 6766.
[12] B. Chen, C. Liang, J. Yang, D. S. Contreras, Y. L. Clancy, E. B. Lobkovsky, O. M. Yaghi, S. Dai, *Angew. Chem. Int. Ed.* **2006**, *45*, 1390.
[13] K. Barthelet, J. Marrot, D. Riou, G. Férey, *Angew. Chem. Int. Ed.* **2002**, *41*, 281.
[14] L. Alaerts, C. E. A. Kirschhock, M. Maes, M. A. v. d. Veen, V. Finsy, A. Depla, J. A. Martens, G. V. Baron, P. A. Jacobs, J. F. M. Denayer, D. E. D. Vos, *Angew. Chem. Int. Ed.* **2007**, *46*, 4293.
[15] B. Wang, A. P. Côte, H. Furukawa, M. O'Keeffe, O. M. Yaghi, *Nature* **2008**, *453*, 207.
[16] S. S. Kaye, A. Dailly, O. M. Yaghi, J. R. Long, *J. Am. Chem. Soc.* **2007**, *129*, 14176.
[17] S. Kitagawa, S.-i. Noro, T. Nakamura, *Chem. Commun.* **2006**, 701.
[18] K. L. Mulfort, J. T. Hupp, *J. Am. Chem. Soc.* **2007**, *129*, 9604.
[19] B. Panella, K. Hönes, U. Müller, N. Trukhan, M. Schubert, H. Pütter, M. Hirscher, *Angew. Chem. Int. Ed.* **2008**, *47*, 2138.
[20] K. Seki, *Phys. Chem. Chem. Phys.* **2002**, *4*, 1968.
[21] B. Kesanli, Y. Cui, M. R. Smith, E. W. Bittner, B. C. Bockrath, W. Lin, *Angew. Chem. Int. Ed.* **2005**, *44*, 72.
[22] B. Chen, S. Ma, F. Zapata, E. B. Lobkovsky, J. Yang, *Inorg. Chem.* **2006**, *45*, 5718.
[23] T. K. Maji, R. Matsuda, S. Kitagawa, *Nat. Mater.* **2007**, *6*, 142.
[24] B. Chen, S. Ma, F. Zapata, F. R. Fronczek, E. B. Lobkovsky, H.-C. Zhou, *Inorg. Chem.* **2007**, *46*, 1233.
[25] S. Ma, X.-S. Wang, E. S. Manis, C. D. Collier, H.-C. Zhou, *Inorg. Chem.* **2007**, *46*, 3432.
[26] B. Chen, S. Ma, E. J. Hurtado, E. B. Lobkovsky, H.-C. Zhou, *Inorg. Chem.* **2007**, *46*, 8490.
[27] B. Chen, S. Ma, E. J. Hurtado, E. B. Lobkovsky, C. Liang, H. Zhu, S. Dai, *Inorg. Chem.* **2007**, *46*, 8705.
[28] S. Ma, X.-S. Wang, D. Yuan, H.-C. Zhou, *Angew. Chem. Int. Ed.* **2008**, *47*, 4130.
[29] M. Xue, S. Ma, Z. Jin, R. M. Schaffino, G.-S. Zhu, E. B. Lobkovsky, S.-L. Qiu, B. Chen, *Inorg. Chem.* **2008**, *47*, 6825.
[30] D. N. Dybtsev, H. Chun, K. Kim, *Angew. Chem. Int. Ed.* **2004**, *43*, 5033.
[31] S.-I. Noro, S. Kitagawa, M. Kondo, K. Seki, *Angew. Chem. Int. Ed.* **2000**, *39*, 2081.
[32] H. J. Buser, D. Schwarzenbach, W. Petter, A. Ludi, *Inorg. Chem.* **1977**, *16*, 2704.
[33] M. V. Bennett, L. G. Beauvais, M. P. Shores, J. R. Long, *J. Am. Chem. Soc.* **2001**, *123*, 8022.
[34] S. Subramanian, M. J. Zaworotko, *Angew. Chem. Int. Ed. Engl.* **1995**, *34*, 2127.
[35] M. J. Zaworotko, *Angew. Chem. Int. Ed.* **2000**, *39*, 3052.
[36] S.-i. Noro, R. Kitaura, M. Kondo, S. Kitagawa, T. Ishii, H. Matsuzaka, M. Yamashita, *J. Am. Chem. Soc.* **2002**, *124*, 2568.
[37] As mentioned in the experimental section, a violet powder (**1b** $\supset 2H_2O$) was obtained after stirring pyz, $Cu(BF_4)_2{\cdot}xH_2O$ and $(NH_4)_2SiF_6$ for one day, whereas two types of powder (blue **1a** and violet **1b** $\supset 2H_2O$) were obtained after stirring for 6 h. X-ray powder diffraction clearly shows their coexistence, as shown in Figure S3.
[38] G. R. Desiraju, *Nat. Mater.* **2002**, *1*, 77.
[39] The size is measured by considering van der Waals radii for constituting atoms. Hereafter, all the size estimations of pores are made in this way.
[40] M. Aoyagi, K. Biradha, M. Fujita, *Bull. Chem. Soc. Jpn.* **2000**, *73*, 1369.
[41] S. Hu, K.-H. He, M.-H. Zeng, H.-H. Zou, Y.-M. Jiang, *Inorg. Chem.* **2008**, *47*, 5218.
[42] S. Horike, D. Tanaka, K. Nakagawa, S. Kitagawa, *Chem. Commun.* **2007**, 3395.
[43] T. Yoshimura, K. Umakoshi, Y. Sasaki, S. Ishizaka, H.-B. Kim, N. Kitamura, *Inorg. Chem.* **2000**, *39*, 1765.
[44] L. R. MacGillivray, S. Subramanian, M. J. Zaworotko, *J. Chem. Soc., Chem. Commun.* **1994**, 1325.
[45] R. D. Gillard, *Coord. Chem. Rev.* **1975**, *16*, 67.
[46] X.-M. Zhang, M.-L. Tong, X.-M. Chen, *Angew. Chem. Int. Ed.* **2002**, *41*, 1029.
[47] J. Tao, Y. Zhang, M.-L. Tong, X.-M. Chen, T. Yuen, C. L. Lin, X. Huangd, J. Li, *Chem. Commun.* **2002**, 1342.
[48] M.-L. Tong, L.-J. Li, K. Mochizuki, H.-C. Chang, X.-M. Chen, Y. Li, S. Kitagawa, *Chem. Commun.* **2003**, 428.
[49] X.-M. Zhang, X.-M. Chen, *Eur. J. Inorg. Chem.* **2003**, 413.
[50] N. Lah, I. K. Cigić, I. Leban, *Inorg. Chem. Commun.* **2003**, *6*, 1441.
[51] Y.-Z. Zheng, M.-L. Tong, X.-M. Chen, *New J. Chem.* **2004**, *28*, 1412.
[52] P. Lumme, S. Lindroos, E. Lindell, *Acta Crystallogr., Sect. C* **1987**, *43*, 2053.
[53] J. Y. Lu, B. R. Cabrera, R.-J. Wang, J. Li, *Inorg. Chem.* **1999**, *38*, 4608.
[54] K. Jin, X. Huang, L. Pang, J. Li, A. Appel, S. Wherland, *Chem. Commun.* **2002**, 2872.
[55] J.-P. Zhang, S.-L. Zheng, X.-C. Huang, X.-M. Chen, *Angew. Chem. Int. Ed.* **2004**, *43*, 206.
[56] C.-Z. Xie, Z.-F. Zhang, B.-F. Zhang, X.-Q. Wang, R.-J. Wang, G.-Q. Shen, D.-Z. Shen, B. Ding, *Eur. J. Inorg. Chem.* **2006**, 1337.
[57] K. Uemura, A. Maeda, H. Kita, *Polyhedron* **2008**, *27*, 2939.
[58] Speck, A. L. PLATON, A. M. C. T. Utrecht University, Utrecht, The Netherlands, **1999**.
[59] R. W. Gable, B. F. Hoskins, R. Robson, *J. Chem. Soc., Chem. Commun.* **1990**, 1677.
[60] M. A. Withersby, A. J. Blake, N. R. Champness, P. A. Cooke, P. Hubberstey, A. L. Realf, S. J. Teat, M. Schröder, *J. Chem. Soc., Dalton Trans.* **2000**, 3261.
[61] T. Sunahara, S. Onaka, M. Ito, H. Imai, K. Inoue, T. Ozeki, *Eur. J. Inorg. Chem.* **2004**, 4882.
[62] B. Li, B. Li, X. He, Y. Zhang, *J. Mol. Struct.* **2004**, *692*, 115.
[63] C. H. Springsteen, R. D. Sweeder, R. L. LaDuca, *Cryst. Growth Des.* **2006**, *6*, 2308.
[64] D. B. Cordes, C. V. K. Sharma, R. D. Rogers, *Cryst. Growth Des.* **2007**, *7*, 1943.
[65] B. Liu, X.-C. Zhang, Y.-F. Wang, *Inorg. Chem. Commun.* **2007**, *10*, 199.

[66] R. A. J. Driessen, F. B. Hulsbergen, W. J. Vermin, J. Reedijk, *Inorg. Chem.* **1982**, *21*, 3594.
[67] M. Conner, A. McConnell, J. Schlueter, J. Manson, *J. Low Temp. Phys.* **2006**, *142*, 273.
[68] M.-C. Suen, Z.-K. Chan, J.-D. Chen, J.-C. Wang, C.-H. Hung, *Polyhedron* **2006**, *25*, 2325.
[69] M.-C. Suen, J.-C. Wang, *Struct. Chem.* **2006**, *17*, 315.
[70] D. N. Dybtsev, H. Chun, S. H. Yoon, D. Kim, K. Kim, *J. Am. Chem. Soc.* **2004**, *126*, 32.
[71] M. Dincă, J. R. Long, *J. Am. Chem. Soc.* **2005**, *127*, 9376.
[72] S. M. Humphrey, J.-S. Chang, S. H. Jhung, J. W. Yoon, P. T. Wood, *Angew. Chem. Int. Ed.* **2007**, *46*, 272.
[73] O. K. Farha, A. M. Spokoyny, K. L. Mulfort, M. F. Hawthorne, C. A. Mirkin, J. T. Hupp, *J. Am. Chem. Soc.* **2007**, *129*, 12680.
[74] Y. Zou, S. Hong, M. Park, H. Chun, M. S. Lah, *Chem. Commun.* **2007**, 5182.
[75] K. M. Ok, J. Sung, G. Hu, R. M. J. Jacobs, D. O'Hare, *J. Am. Chem. Soc.* **2008**, *130*, 3762.
[76] J. A. R. Navarro, E. Barea, A. Rodriguez-Dieguez, J. M. Salas, C. O. Ania, J. B. Parra, N. Masciocchi, S. Galli, A. Sironi, *J. Am. Chem. Soc.* **2008**, *130*, 3978.
[77] M. E. van Leeuwen, *Fluid Phase Equilib.* **1994**, *99*, 1.
[78] M. M. Dubinin, *Chem. Rev.* **1960**, *60*, 235.
[79] The Dubinin–Radushkevich (DR) equation was used to analyze the resulting isotherms and to characterize the porous properties of **2**. The DR equation is given by $\ln W = \ln W_0 + (A/\beta E_0)^2$, where W and W_0 are the amount adsorbed at a relative pressure (P/P_0) and the saturation adsorption, respectively. E_0 is a characteristic adsorption energy, and the parameter A is Polanyi's adsorption potential, defined as $A = RT \ln(P_0/P)$. The parameter β is the affinity coefficient and is related to the adsorbate–adsorbent interaction.
[80] A. J. Fletcher, E. J. Cussen, D. Bradshaw, M. J. Rosseinsky, K. M. Thomas, *J. Am. Chem. Soc.* **2004**, *126*, 9750.
[81] The double exponential (DE) equation is described as $M_t/M_e = A_1(1 - \exp(-k_1t)) + A_2[1 - \exp(-k_2t)]$, where k_1 and k_2 are kinetic rate constants and A_1 and A_2 are the relative contributions of the two barriers controlling the overall process, with $A_1 + A_2 = 1$.
[82] B. Chen, X. Zhao, A. Putkham, K. Hong, E. B. Lobkovsky, E. J. Hurtado, A. J. Fletcher, K. M. Thomas, *J. Am. Chem. Soc.* **2008**, *130*, 6411.
[83] A log plot of H_2 adsorption/desorption isotherms at 298 K, which shows that the desorption isotherm does not retrace the adsorption isotherm, is shown in Figure S10.
[84] G. Férey, M. Latroche, C. Serre, F. Millange, T. Loiseau, A. Percheron-Guégan, *Chem. Commun.* **2003**, 2976.
[85] X. Zhao, B. Xiao, A. J. Fletcher, K. M. Thomas, D. Bradshaw, M. J. Rosseinsky, *Science* **2004**, *306*, 1012.
[86] H. J. Choi, M. Dincă, J. R. Long, *J. Am. Chem. Soc.* **2008**, *130*, 7848.
[87] J. Y. Lee, J. Li, J. Jagiello, *J. Solid State Chem.* **2005**, *178*, 2527.
[88] P. M. Forster, J. Eckert, B. D. Heiken, J. B. Parise, J. W. Yoon, S. H. Jhung, J.-S. Chang, A. K. Cheetham, *J. Am. Chem. Soc.* **2006**, *128*, 16846.
[89] C. Yang, X. Wang, M. A. Omary, *J. Am. Chem. Soc.* **2007**, *129*, 15454.
[90] Higashi, T. *Abscor – Empirical Absorption Correction based on Fourier Series Approximation*, Rigaku Corporation, Tokyo, Japan **1995**.
[91] *SHELXTL Reference Manual*, ver. 5.1, Bruker AXS, Analytical X-ray Systems, Madison, WI, **1997**.

Received: February 11, 2009
Published Online: April 8, 2009

